

Solar Evaporation via Nano-Fluids: A Comparative Study

D.Navilan

Lecturer (Selection Grade), Department of Physics, Sankar Polytechnic College, Sankarnagar, Tirunelveli

Abstract- Vaporization (evaporation and boiling) through direct absorption solar collectors (DASCs) has recently drawn significant attention. Many studies suggested that plasmonic nanoparticles, such as gold nano-particles, can significantly enhance the photo-thermal conversion efficiency of DASCs. However, there is still a lack of comparative studies of the feasibility of using gold nanoparticles for solar applications. This study performed well-controlled experiments for two different categorized particles, i.e., gold and carbon black suspended in water, and assessed their performance in terms of evaporation rate, materials cost and energy consumption. The results show that gold nanofluids are not feasible for solar evaporation applications, where the cost of producing 1 g/s vapor is ~300 folds higher than that produced by carbon black nanofluids. This infeasibility is mainly due to the high cost and the low absorbance of gold comparing to carbon black nanoparticles. Moreover, this work reveals that with the increase of nano-particle concentration or incident solar radiation, more energy is trapped in a small volume of the nanofluid near the interface, resulting in a local higher temperature and a higher evaporation rate. For efficient steam production, future optimization of the system should consider concentrating more solar energy at the interface to maximize the energy consumed for evaporation.

Index Terms- Direct Absorption, Nano Fluid, Solar Energy, Solar Evaporation and Economic Analysis.

I. INTRODUCTION

Developing efficient and economically feasible renewable energy conversion technologies is essential to address our imminent problems such as environment pollution, fossil fuel depletion and population increase. Solar energy has been claimed as the energy of our future. However, challenges such as high cost (due to using optical devices such as heliostats or reflectors to concentrate the solar energy, tracking devices to track the energy source, and vast land for installation) and low efficiency (due

to the heat losses) of solar energy conversion systems [1e3] limit their wide applications.

Nanoparticle-based direct absorption solar collectors (DASCs), which utilize the high radiation absorption property of nano-particles suspended in a working fluid, are proposed to increase the efficiency of solar systems. Since the proposition of this method, enormous efforts by research groups around the world have been spent to investigate the effects of nanoparticles' composition, size, and shape on the photo-thermal conversion efficiencies of these DASCs [4e8].

Recently, DASCs have been proposed as novel solar-driven steam generation systems [3], and using gold nanofluids has attracted intense interest [9e15], albeit they are among the most expensive materials. This interest comes from two main reasons: Firstly, most of the solar working fluids are semi-transparent for the visible spectrum, which represents ~40% of the solar energy, and the resonance of the conducting electrons of gold nanoparticles can be tuned so that the peak absorbance occurs in the visible spectrum. As the enhancement in the light absorption has unavoidably a narrow bandwidth of the wavelength [16], this promotes the use of hybrids of different sizes and/or shapes of gold nanoparticles to broaden the bandwidth of the absorption peak [16e19]. However, a reduction in the peak absorption value necessarily occurs due to the dilution of gold nanofluids at a given total particle concentration, according to the Beer's law. This means a higher concentration of gold nanoparticles is needed to prepare a hybrid with a broad bandwidth at the same peak value of absorbance. Secondly, the claim of nano bubbles generation around immersed nanoparticles can enhance the efficiency of solar-driven steam generation, albeit the bulk temperature of a nanofluid is still sub cooled [15,20,21], is still subjecting to strong debate. It has been suggested that nano-bubbles can only be generated under very high intensity of light, i.e., of thousands of kW/m²

[13,22e24], which consequently requires expensive optical and tracking devices.

Many studies assumed a uniform temperature distribution within a nanofluid although the effect of the optical path was not negligible, and one temperature was used to analyse the photo-thermal conversion efficiency [12,15,21,25e28]. However, the Non-linearly reduction in the radioactive intensity along the depth of the nanofluid should cause large temperature gradient within the nanofluid [13,29]. Neglecting this temperature gradient will lead to an inaccurate analysis of the results such as over-estimation of the solar evaporation efficiency or under-estimation of the energy stored in the bulk nanofluid. Moreover, most of the published work was based on only one particular type of particles, and a comparative assessment of the performance of commonly used nano- materials for solar-driven steam generation is still lacking. The effect of these nanomaterials needs to be investigated at the same concentration and under similar operating conditions to reach a fair comparison [3]. In addition to the efficiency, the cost must be considered very carefully for any practical application. For the purpose of comparison, some estimation of the cost of a unit steam generation rate (\$/g/s) from different nanoparticles is preferred.

This study aims to clarify the mechanism of the solar steam generation and to investigate the feasibility of using gold nano- particles under low concentrations of solar radiation (10 Suns). By performing well-controlled experiments, a comparison between aqueous gold (Au) and carbon black (CB) nanofluids was conducted. Evaporation rate, cost of a unit steam rate generation (\$/g/s), and energy consumption were calculated from the recorded transient temperature rise and mass change of the nanofluids. Furthermore, more experiments were conducted to investigate the effect of the incident solar radiation intensity on the temperature distribution within the nanofluids.

II. PREPARATION OF NANOFLUIDS

2.1. Synthesis of gold nanofluid

In this study, gold nanofluid (Au) was synthesized by the citrate reduction method as reported by Chen and Wen [30] and Zhang et al. [31]. Typically, 100 ml of 5 mM HAuCl₄ solution was mixed with 100 ml of 10 mM tri-sodium citrate solution. Then, the resultant

mixture was heated to the boiling temperature until its color became wine red. After that, the resultant was put into a sonication bath at 80 °C for 3 h. The synthesized gold nanoparticles were left for 24 h at the room temperature and then purified by the membrane dialysis method. In this process, the gold nanofluid was put in a membrane tube with a pore size of 2e3 nm in diameter to allow a smooth diffusion of ions and keep the gold nanoparticles inside the tube. The membrane tube was placed in a beaker filled with deionized (DI) water of 2000 ml and stirred by a magnetic stirrer. The DI water was changed twice a day for ten days.

2.2. Preparation of carbon black nanofluid

Carbon black (CB) nanofluid was prepared by the two-step method, i.e. by dispersing a certain amount of presynthesised nanopowder to a hosting liquid, i.e., deionized (DI) water in this work. The carbon black nanopowder was purchased from Alfa Aesar (CAS# 1333-86-4, purity 99.9%, average particle size 42 nm, S.A. 75 m²/g, bulk density 80e120 g/l and density 1.8e2.1 g/cm³ @ 20 °C). Since Tween compounds are widely used as surfactants, emulsifiers and wetting agents [32,33], it is common to use them in stabilizing nanofluids. Tween®80 was purchased from Sigma Aldrich. Tween was added to DI water at 0.02 vol %, and the hosting liquid was magnetically stirred when controlled amount of nanopowder was added. After 15 min, the sample was put into an ultra-sonication bath (Fisher Scientific, 750 W power) for 30 min, followed by a powerful probe sonication (Fisher Scientific, 700 W power, and 20 kHz frequency) for extra 30 min, i.e. 80 W for 5 min, followed by 5 min for cooling down the sample, and followed by another 80 W, 5 min sonication, and so on.

III. CHARACTERIZATION

A flame atomic absorption spectrometer (AAS) was used to measure the concentration of prepared gold nanofluid, which turned out to be 250 mg/l. Different dilutions (25, 50, and 100 mg/l) were prepared from the stock nanofluid, as shown in Fig. 1 and Table 1. A UV-Vis Spectrophotometer (UV-1800, Shimadzu Corporation, Japan) was used to measure the capability of radiation absorption of gold and carbon black dilutions. The absorption spectra are shown in figures. The results reveal an excellent agreement

between the absorbance results and the Beer's law, which indicates a linear relationship between absorbance and solution concentration, as shown in the insets of the two figures. The slope of the absorbance line of the gold nanofluids is 0.011=cm, while it is 0.029 l=cm for the carbon black nanofluids. It is clear that gold nanofluids have good absorbance in the range of 300e600 nm wavelength and the peak value is around 528 nm, which is due to the local surface Plasmon resonance. However, the absorption capability of the carbon black nanofluids is better than the gold nanofluids over the measuring spectrum. As the absorbance of a nanofluid depends on the size and shape of the nanoparticles, the spectrophotometer was used to examine the nanofluid stability [34]. Negligible changes were detected on the absorbance of the prepared nanofluids after a week of storing on shelf. Moreover, the Zeta-potential and hydrodynamic nanoparticle size distribution were measured by a Malvern Zetasizer (NanoZS90 5001). The Zeta- potentials were $(37.6 \pm 0.7 \text{ mV})$ and $(32.3 \pm 1 \text{ mV})$ for gold and carbon black nanofluids respectively, which revealed good stability.

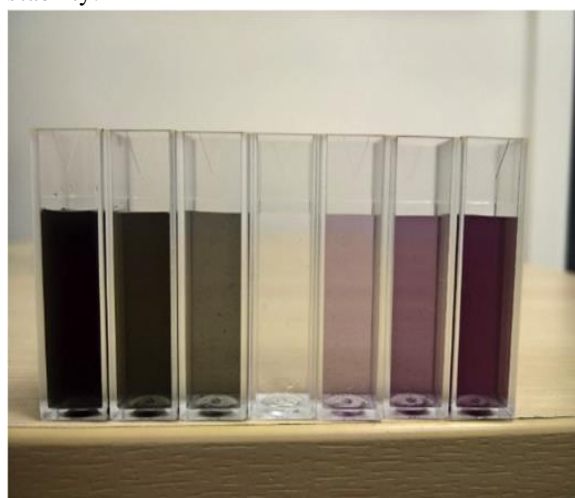


Figure 1: Picture of gold and carbon black nanofluid dilutions. The mid sample is DI water, to the right are gold nanofluids and to the left are carbon black nanofluids. The concentrations are 25, 50, and 100 mg/l respectively.

The size distribution measurements, relying on the dynamic light scattering (DLS), showed a polydisperse gold nanoparticles with a polydispersity index (PdI) of 0.447 and average diameter of $36.18 \pm 24.18 \text{ nm}$. Two peaks of scattering intensity were detected. One of 86.1% of

the intensity at $66.82 \pm 30.91 \text{ nm}$, and the other of 13.9% of the intensity at $8.88 \pm 2.65 \text{ nm}$. Fortunately, since the scattering light intensity is related to the nanoparticle's diameter to power six, most the nanoparticles' primary size is less than 10 nm, this comparison shows the danger of relying on purely TEM or SEM

mg/l (ppm)	Wt. %	Vol. % for Au nanofluid	Vol. % for CB nanofluid
25	0.0025	0.000129	0.00125
50	0.0050	0.000259	0.0025
100	0.0100	0.000518	0.005

Table 1: Concentration of the nanofluids in different forms.

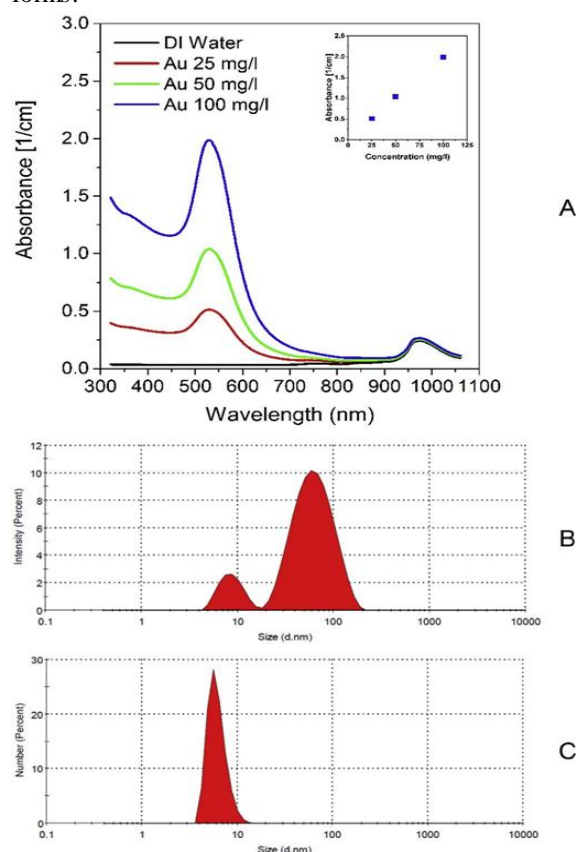
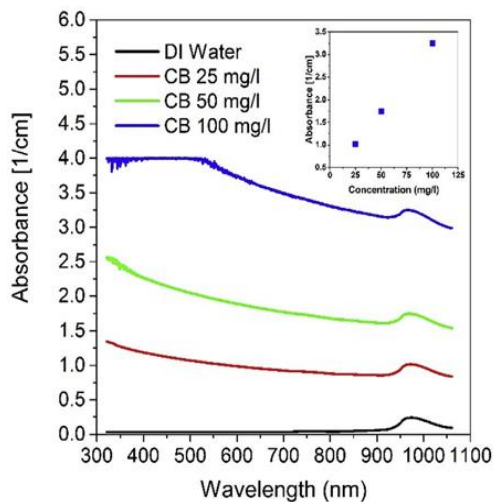
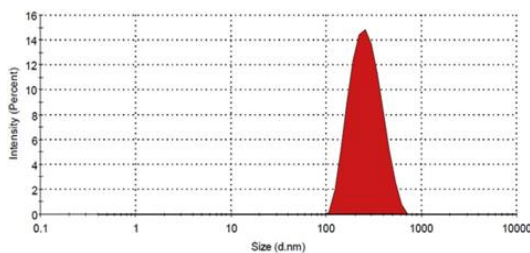


Figure 2: Spectrum absorbance (A), and the particle size distribution (B) as a function of DLS, (C) as a function of nanoparticles number of gold nanofluids. for nanoparticle characterization. However, one peak of the scattering light intensity was detected from the carbon black nanofluid at $272.6 \pm 100.9 \text{ nm}$. The average size was $244.9 \pm 93.57 \text{ nm}$ (see Fig. 3(B) and (C)). A transmission electron microscope (TEM, FEI Tecnai TF20) was used to examine the shape and size of the nanoparticles. The synthesised gold

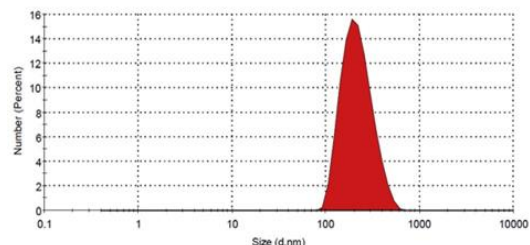
nanoparticles had different shapes (spherical, oval, and triangular) and sizes (small and large) While big clusters of carbon black nano- particles The TEM results interpret the DLS results well.



A



B



C

Figure 3: Spectrum absorbance (A), and the particle size distribution (B) as a function of DLS, (C) as a function of nanoparticles number of carbon black nanofluids.

IV. SOLAR EVAPORATION EXPERIMENTAL SETUP

The photo-thermal conversion experimental setup is shown in Figure. A solar simulator (ORIEL® I3A™, Xenon Arc Lamp, Class AAA Solar simulator) was used as a light source to minimize the uncertainties under direct sunlight. This solar simulator provides a radiation spectrum match the solar spectra, and the intensity can be varied by using suitable filters. This

device is certified to IEC 60904-9 2007 edition, JIS C 8912 and ASTM E 927-05 standards.

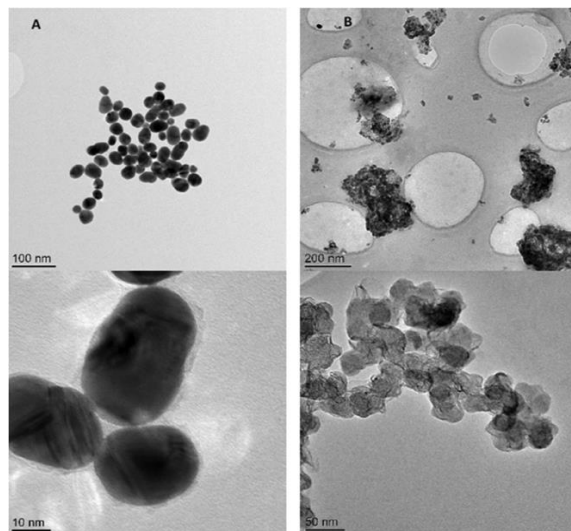


Figure 4: TEM images of (A) gold and (B) carbon black nanoparticles.

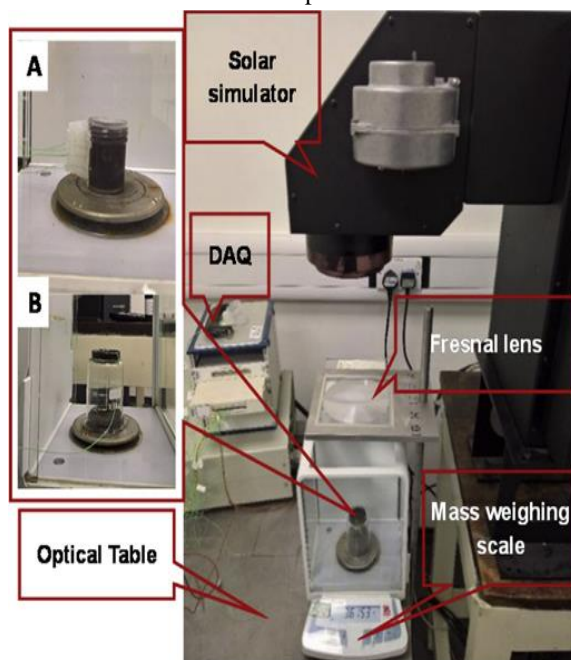


Figure 5: Solar evaporation experimental setup. (A) 45 ml sample and (B) 4 ml sample containers

The performance parameters of the sun simulator are: spectral match between 0.75 and 1.25% of the solar spectrum, non-uniformity < 2% and temporal instability < 0.5%. A FLIR ONE infrared camera (sensitivity of 0.1 °C) to detect the temperature distribution within the nanofluids, a Fresnel lens (Edmund Optics) with a 250 mm focal distance to focus the source light, and a digital

weighing scale (Ohaus Discovery, a precision of ± 0.1 mg) to measure the samples' mass change were used. Two containers were utilized in this study: A cylindrical one of 35 mm diameter and 40 mm height was used to get the temperature distribution within the nanofluids using the infrared camera. While the other one was a Petri dish of 35 mm diameter. By using precise micro-pipettes, 45 ml sample was put in the cylindrical container, and a 4 ml sample was put in the Petri dish to form a thin layer of the nanofluid (~ 4 mm) to minimize the temperature gradient within the sample. The Petri dish was placed on the bottom of an upside down glass beaker in the center spot of the solar simulator. Uniform temperature distribution at the same depth was found by preliminary tests using multiple thermocouples. To minimize the influence of thermocouples in a 4-ml volume, only one K-type thermocouple (Omega 5TC-TT-K-36-36, a diameter of 0.13 mm and a precision of ± 0.5 K) was used to measure the temperature of the center of the sample. The transient data (mass and bulk temperature) was recorded to a PC via a data acquisition system under the Lab VIEW environment. The experimental setup, except the solar simulator, was located on a stable optical table to minimize the vibration effect on the readings, and the experiments were performed in an isolated (i.e., the disturbance and noise were kept to the minimum) and well controlled lab (the temperature and humidity were within 1°C and 2% respectively). Preliminary tests with five thermocouples located at different positions on the bottom of the Petri dish showed that the space variation of the sample temperature was negligible. Moreover, the photo-thermal conversion experiment was repeated three times for each sample. The standard deviation was found ≤ 0.5 K for temperature and ≤ 0.1 mg for mass measurements.

V. RESULTS AND DISCUSSIONS

5.1. Experiment with 45 ml samples

To demonstrate qualitatively the effect of nanoparticles concentration on the solar radiation absorption, temperature distribution within the bulk fluid and evaporation rate, experiment was conducted on 45 ml volume samples by using gold nanofluids (0, 25, 50, and 100 mg/l) subjected to a radiation (heating-up) from the solar simulator (10 kW/m²) for

900 s and continued for another 900 s without radiation (cooling-down). A FLIR ONE infrared thermal camera (0.1 K sensitivity) was positioned 50 cm far from the sample to capture the temperature distribution within the nano-fluid's depth each 60 s and a precise mass scale (Ohaus Discovery, 0.1 mg sensitivity) was used to measure the mass change each 1 s. The results are shown in Table 2. It is clear that adding nanoparticles to water makes the temperature distribution highly non-homogeneous during the heating-up process under the solar simulator light. With the increase of nanoparticles concentration, the hottest layer of the nanofluid becomes thinner and closer to the interface between the gaseous and liquid phases, resulting in a higher evaporation rate. Also, it is clear that a thin layer of nanofluid is needed to minimize the non-homogeneity in the temperature. Therefore, a small volume of the nanofluids was used to investigate the feasibility of using gold nanofluids in solar evaporation applications, as in section 5.2. However, the temperature distribution gradually becomes homogenous during the cooling-down process, i.e. under no radiation.

These results can be interpreted by the Beer's law, which relates the transmitted radiation to the material properties through which the radiation is passing according to:

$$T(\lambda) = \frac{I(\lambda)}{I_0(\lambda)} = e^{-\alpha(\lambda, f)y}$$

where $T(\lambda)$ is the spectral transmittance; $I(\lambda)$ is the spectral transmitted light intensity @ y ; $I_0(\lambda)$ is the incident spectral light intensity @ $y = 0$; $\alpha(\lambda, f)y$; f is the extinction coefficient; y is the light path and f is the nano fluid's concentration.

It is obvious that the energy absorbed is exponentially proportional to the extinction coefficient, which is a function of nano-fluid's concentration, and the length of the light path (y). Moreover, the rate change of the absorbed energy with respect to depth is a function of the incident light intensity in addition to the extinction coefficient and depth.

Assuming constant spectral extinction coefficient, the solution of Eq. (4). As the evaporation process is a surface phenomenon; it is preferred to trap most of the solar energy in a very thin layer of the nanofluid to maximize the evaporation efficiency. However, it

is obvious that to achieve this goal, high extinction coefficient is needed. For instant, extinction coefficient of 24 is required to absorb 90% of the incident energy, and assuming that Beer's law is still applicable (i.e., Beer's law is applicable for dilute solutions), performing linear extrapolation reveals that the corresponding concentration is 830 mg/l. It is expected that the concentration of gold nanofluid must be higher than 830 mg/l due to its low absorbance comparing to carbon black. Such a high concentration might prevent utilizing gold nanofluids in solar applications that need to high volume of working fluids.

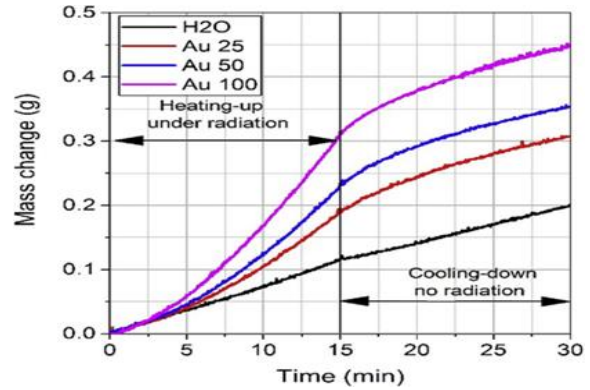


Figure 6: The temporary mass change of different concentrations of gold nanofluids

Time [min]	Au 0 mg/l	Au 25 mg/l	Au 50 mg/l	Au 100 mg/l
Initial stage				
Heating-up under solar radiation	5:	5:	5:	5:
	10:	10:	10:	10:
	15:	15:	15:	15:
	20:	20:	20:	20:
Cooling-down (no radiation)	25:	25:	25:	25:
	30:	30:	30:	30:

Table 2: Temperature distribution within different concentration of gold nanofluids. The samples are subjected to 10 kW/m² radiation for the first 15 min

(heating-up process), after that samples go through a cooling-down process (No radiation).

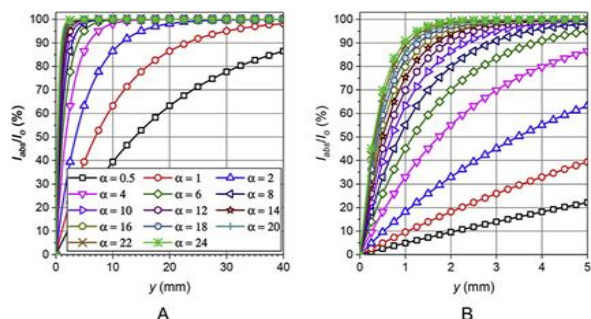


Figure 7: The absorbed energy portion as a function of the nanofluid's depth and extinction coefficient. The rate change of the absorbed light intensity with respect to the nanofluid's depth as a function of the incident light intensity, which represents the solution of Eq. (5), assuming unity extinction coefficient. It is clear that the initial light intensity has a significant effect on the dI_{abs}/dy value. As the initial incident light increases, the slope of dI_{abs}/dy increases when $y/0$. In other words, more energy is absorbed near the interface between the liquid and gaseous phases when the incident light is increased. As a result, it is expected that the highest temperature is near the interface. To justify this expectation, a photo-thermal conversion experiment was performed using carbon black nanofluid (CB 25 mg/l) under different light intensity, i.e. 1, 2.5, 5 and 10 Suns. The temperature distribution within the nanofluid was recorded via 4 K-type thermocouples (Omega 5TC-TT-K-36-36, a diameter of 0.13 mm and a precision of ± 0.5 K) positioned at the center of the sample at different depth from the air-nanofluid interface. Indeed the temperature decreases nonlinearly as the position goes deeper in the nanofluid during the heating-up under the incident radiation and the best fitting expression for this temperature decay. This nonlinear decay becomes more obvious when the intensity increases. The trend of the temperature distribution lines suggests that the temperature near the interface is the highest. While during the cooling-down process (no radiation), it is clear that the temperature becomes lower near the interface than the other positions in the nanofluid, which is due to the heat loss to the surrounding by evaporation and convection.

5.2. Experiment with 4 ml samples

In this section, a comparative examination between gold (expensive) and carbon black (cheap) nanofluids has been conducted quantitatively. A 4 ml gold or

carbon black nanofluid sample was put in the 35 mm Petri dish making ~ 4 mm thin layer under a solar radiation of 10 kW/m^2 for 600 s. During this period, the samples' temperature and mass were recorded. It is evident that the temperature and mass change trends are the same for both carbon black and gold nanofluids. Only the values are different, and this depends on the light absorption characteristics. Both the temperature and the evaporated mass of the carbon black nanofluids are higher than that of gold nanofluid, which is consistent with the absorbance characteristics.

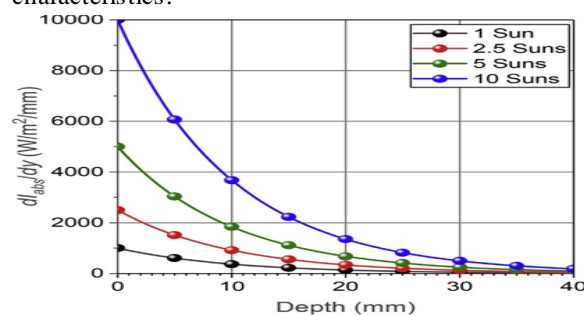


Figure 8: The rate change of the absorbed energy with respect to nano fluid's depth at different incident light intensity

The evaporation rate, the numerical differentiation of the mass change with time, as a function of time and temperature at different nanoparticle concentrations for gold and carbon black nanofluids respectively. It is noted that for both samples, the evaporation rate is higher during the heating-up period than the cooling-down period at the same temperature reading, and this difference becomes more significant as the nanoparticles concentration becomes higher. As the evaporation rate is proportional to the kinetic energy of the water molecules at the interface between the gaseous and liquid phases, this difference shall be related to the interface temperature difference between the heating-up and cooling-down periods as the rate change of the absorbed energy with respect to the sample depth is an exponential function and this difference increases as the nanofluid's extinction coefficient increases. It shall be noted that the thermocouple is located 2 mm beneath the interface between air and the nanofluid sample. Therefore, even the measured fluid temperature is the same, the interface temperature during the heating-up shall be higher than that during the cooling-down processes and consequently, a higher evaporation rate is expected during the heating-up period.

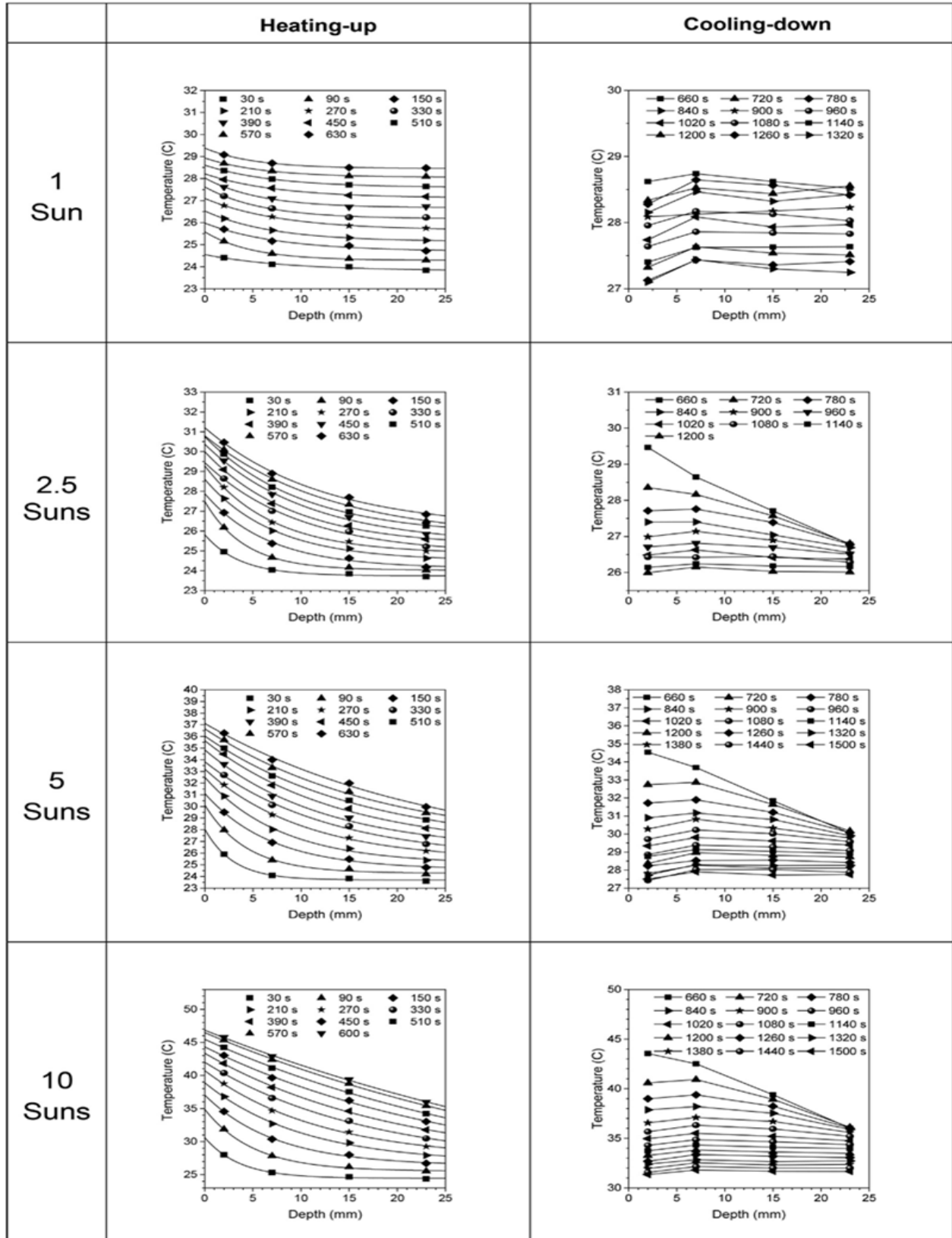


Figure 9: The effect of the incident light intensity on the temperature distribution during heating-up (symbols for the experimental data and the lines are trend lines) and cooling- down of a nanofluid at different Depth time steps.

In addition, one can see that the evaporation rate of different nanofluid concentrations is the same during the cooling-down period at temperatures below 35 °C. This is consistent with the temperature measurement in Fig. 10, where the temperatures of all concentrations become the same after time ~1100 s. As a result, it can be concluded that the effect of the nanoparticles is just to enhance the radiation absorption properties. To enhance the evaporation rate, a better approach is to trap most of the solar energy near the surface, which requires very high nanoparticle concentrations. That will raise problems such as nanoparticles' instability, viscosity increase, and cost increase.

To investigate the feasibility of using gold nanofluids in solar evaporation applications, the cost of producing 1 g/s of water vapour was calculated as:

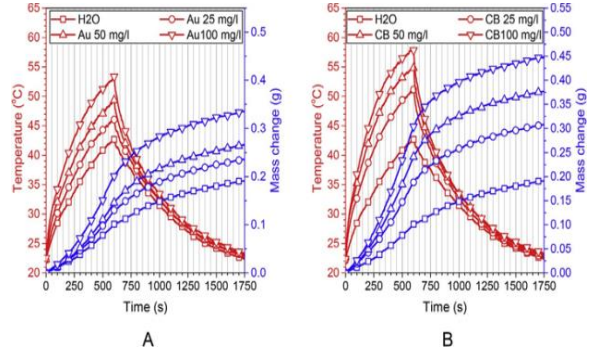


Figure 10: Transient temperature and mass change for (A) gold and (B) carbon black nanofluids

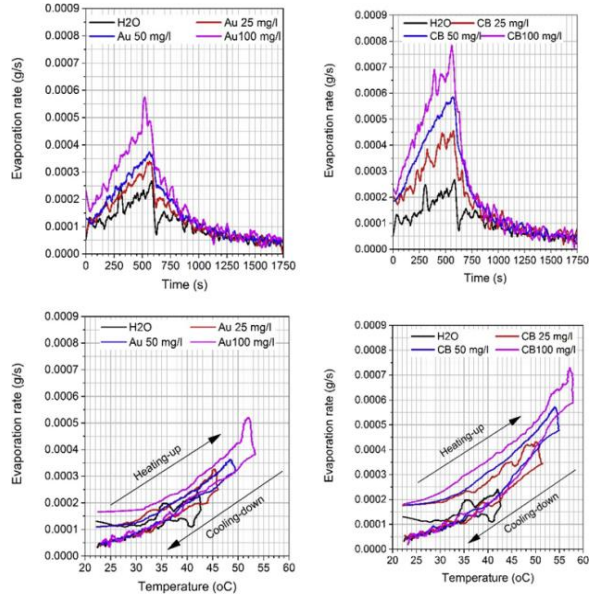


Figure 11: Evaporation rate for gold and carbon black nanofluids as function of time and temperature respectively

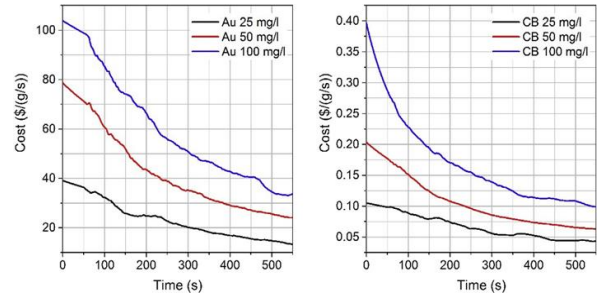


Figure 12: The transient cost of producing 1 g/s of vapour using gold and carbon black nanofluids

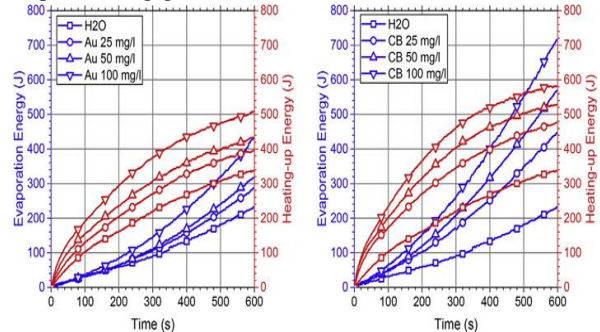


Figure 13: The transient energy consumption for gold and carbon black nanofluids.

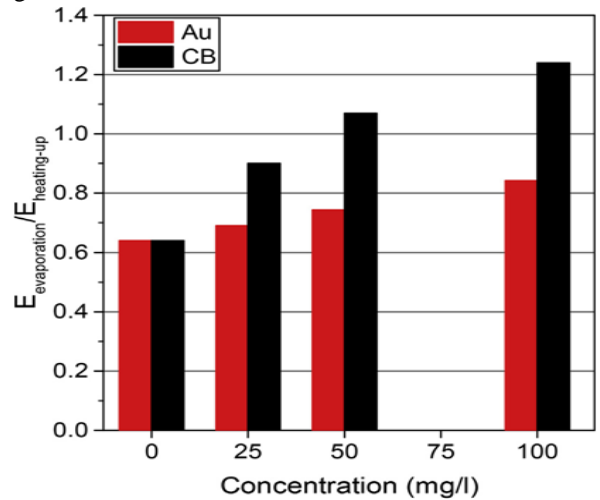


Figure 14: The ratio of energy consumed by evaporation to the energy stored in the nanofluids at time 1/4 600 s.

The thermo physical properties of the nanofluids can be assumed as the same of water because the maximum volumetric concentration is 0.000518% and 0.005% for gold and carbon black nanofluids respectively [28,31,39,40]. The specific heat capacity of water was assumed constant and equal to 4.183 J/gK. This assumption is due to the specific heat capacity of water changes negligibly, i.e. between 4.182 J/gK at 20° C and 4.185 J/gK at 60° C

[41]. While a linear fit with r^2 of 0.9998 was used for Hugli as a function of temperature. The results are shown in Figs. 13 and 14. It is clear that the energy used for evaporation by carbon black nanofluids is ~ 1.64 times higher than that consumed by gold nanofluids. The latent heat to sensible heat ratio is also higher for carbon black nanofluids and such a ratio increases as the concentration increases.

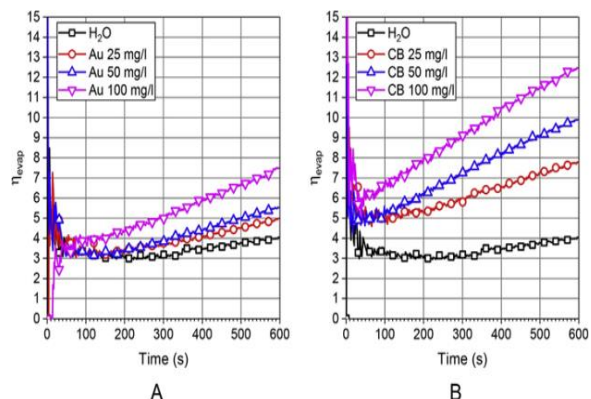


Figure 15: Transient evaporation efficiency as a function of nanofluid's concentration for (A) gold and (B) carbon black nanofluids.

The temporary evaporation efficiency, i.e. energy consumed by evaporation to the total incident energy, as a function of nanofluid's concentration. It is obvious that the evaporation efficiencies of carbon black nanofluids is higher than that of gold nanofluids, which is due to the better solar absorption of carbon black than gold nanofluids. The evaporation efficiency increases as the time increases because of the temporal temperature increase. However, the photo-thermal conversion efficiency (PTE), i.e., the ratio of the sum of evaporation energy (latent heat) and the energy stored in the nanofluid (sensible heat) to the total incident energy, decreases as time increases. This reduction in PTE is due to increased heat losses by convection and radiation. At the first stage, i.e. time ~ 0 s, the increase in the nanofluid's temperature is negligible. Therefore, the heat loss is almost zero. As the time increases, the nanofluid's temperature increases, and consequently the heat loss by convection and radiation increases. As a result, the rate of storing energy in the nanofluid (sensible heat) decreases as time increases, and finally the PTE decreases. Both evaporation process and heat loss by convection and radiation depends on the surface area and temperature. Increasing the nanofluid's surface area and temperature enhances the evaporation rate, but also increases the heat loss.

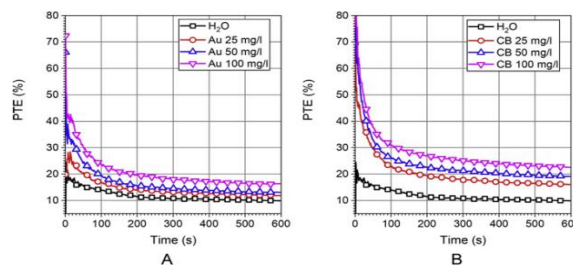


Figure 16: Transient phot-thermal conversion efficiency as function of nanofluid's concentration for (A) gold and (B) carbon black nanofluids.

VI. CONCLUSION

This work investigated the evaporation mechanism of aqueous gold and carbon black nanofluids subjected to concentrated solar radiation. Experiments were conducted using a AAA-rated top class solar simulator to minimize the uncertainties accompanied with natural solar radiation. It was found that:

- The higher the concentration of the nanoparticles or the higher the incident light intensity is, the more solar energy is trapped in a slim volume near the air-nanofluid interface, leading to a higher interface temperature, and consequently higher evaporation rate. This trend is consistent with the Beer's law, which indicates that the absorbed radiation energy is an exponential function of the extinction coefficient that related to nano- particles concentration and light path length.
- The ratio of energy consumed for evaporation to the energy stored in a nanofluid increases with the increase of nanoparticle concentration.
- To enhance the solar evaporation rate, higher nanoparticle concentrations are required to trap more solar energy in a very thin layer, especially for focused solar radiation. This will raise many problems such as the instability of the nanoparticles, the change of physio-thermal properties of the nanofluids, and the high cost as the most of the nanoparticles are in the bulk volume without contributing to evaporation directly.
- Gold nanofluids are found not feasible for solar evaporation applications due to the high cost and low radiation absorbance especially for the wavelengths longer than 600 nm; while carbon black nanofluids are cheaper and more efficient.

REFERENCES

- [1] T.P. Otanicar, et al., Nanofluid-based direct absorption solar collector, *J. Renew. Sustain. Energy* 2 (3) (2010) 033102.
- [2] H.K. Gupta, G.D. Agrawal, J. Mathur, An experimental investigation of a low temperature Al₂O₃-H₂O nanofluid based direct absorption solar collector, *Sol. Energy* 118 (2015) 390e396.
- [3] Z. Deng, et al., An emergence of solar thermal utilization: solar-driven steam generation, *J. Mater. Chem.* 5 (17) (2017) 7691e7709.
- [4] P. Phelan, et al., Trends and opportunities in direct-absorption solar thermal collectors, *J. Therm. Sci. Eng. Appl.* 5 (2) (2013) 021003.
- [5] K. Leong, et al., An overview on current application of nanofluids in solar thermal collector and its challenges, *Renew. Sustain. Energy Rev.* 53 (2016) 1092e1105.
- [6] F. Javadi, R. Saidur, M. Kamalisarvestani, Investigating performance improvement of solar collectors by using nanofluids, *Renew. Sustain. Energy Rev.* 28 (2013) 232e245.
- [7] A. Kasaeian, A.T. Eshghi, M. Sameti, A review on the applications of nanofluids in solar energy systems, *Renew. Sustain. Energy Rev.* 43 (2015) 584e598.
- [8] O. Mahian, et al., A review of the applications of nanofluids in solar energy, *Int. J. Heat Mass Tran.* 57 (2) (2013) 582e594.
- [9] Y. Fu, et al., Investigation on enhancing effects of Au nanoparticles on solar steam generation in graphene oxide nanofluids, *Appl. Therm. Eng.* 114 (2017) 961e968.
- [10] M. Amjad, et al., Volumetric solar heating and steam generation via gold nanofluids, *Appl. Energy* 206 (2017) 393e400.
- [11] L. Zhou, et al., Self-assembly of highly efficient, broadband plasmonic absorbers for solar steam generation, *Sci. Aff.* 2 (4) (2016), e1501227.
- [12] O. Neumann, et al., Combining solar steam processing and solar distillation for fully off-grid production of cellulosic bioethanol, *ACS Energy Lett.* 2 (2016) 8e13.
- [13] H. Jin, et al., Steam generation in a nanoparticle-based solar receiver, *Nano Energy* 28 (2016) 397e406.
- [14] K. Bae, et al., Flexible thin-film black gold membranes with ultrabroadband plasmonic nanofocusing for efficient solar vapour generation, *Nat. Commun.* 6 (2015).
- [15] O. Neumann, et al., Solar vapor generation enabled by nanoparticles, *ACS Nano* 7 (1) (2012) 42e49.
- [16] J. Jeon, S. Park, B.J. Lee, Analysis on the performance of a flat-plate volumetric solar collector using blended plasmonic nanofluid, *Sol. Energy* 132 (2016) 247e256.
- [17] J. Jeon, S. Park, B.J. Lee, Optical property of blended plasmonic nanofluid based on gold nanorods, *Optic Express* 22 (104) (2014) A1101eA1111.
- [18] B.J. Lee, et al., Radiative heat transfer analysis in plasmonic nanofluids for direct solar thermal absorption, *J. Sol. Energy Eng.* 134 (2) (2012) 021009.
- [19] J.R. Cole, N. Halas, Optimized plasmonic nanoparticle distributions for solar spectrum harvesting, *Appl. Phys. Lett.* 89 (15) (2006) 153120.
- [20] A. Polman, Solar steam nanobubbles, *ACS Nano* 7 (1) (2013) 15e18.
- [21] O. Neumann, et al., Compact solar autoclave based on steam generation using broadband light-harvesting nanoparticles, *Proc. Natl. Acad. Sci. Unit. States Am.* 110 (29) (2013) 11677e11681.
- [22] G. Baffou, et al., Super-heating and micro-bubble generation around plasmonic nanoparticles under cw illumination, *J. Phys. Chem. C* 118 (9) (2014) 4890e4898.
- [23] S.V. Boriskina, H. Ghasemi, G. Chen, Plasmonic materials for energy: from physics to applications, *Mater. Today* 16 (10) (2013) 375e386.
- [24] P.F. Phelan, et al., Light-induced energy conversion in liquid nanoparticle suspensions, in: W.J.M.E.M.S.J.P. Abraham (Ed.), *Nanoparticle Heat Transfer and Fluid Flow*, CRC Press, Taylor & Francis Group, 2013.
- [25] T. Yousefi, et al., An experimental investigation on the effect of Al₂O₃-H₂O nanofluid on the efficiency of flat-plate solar collectors, *Renew. Energy* 39 (1) (2012) 293e298.
- [26] Q. He, et al., Experimental investigation on photothermal properties of nanofluids for direct

- absorption solar thermal energy systems, *Energy Conv- ers. Manag.* 73 (2013) 150e157.
- [27] E.P. Bandarra Filho, et al., Experimental investigation of a silver nanoparticle- based direct absorption solar thermal system, *Energy Convers. Manag.* 84 (2014) 261e267.
- [28] M. Chen, et al., An experimental investigation on sunlight absorption char- acteristics of silver nanofluids, *Sol. Energy* 115 (2015) 85e94.
- [29] H. Jin, et al., Photothermal conversion efficiency of nanofluids: an experi- mental and numerical study, *Sol. Energy* 139 (2016) 278e289.
- [30] H.-J. Chen, D. Wen, Ultrasonic-aided fabrication of gold nanofluids, *Nanoscale Res. Lett.* 6 (1) (2011) 1e8.
- [31] H. Zhang, et al., Photothermal conversion characteristics of gold nanoparticle dispersions, *Sol. Energy* 100 (2014) 141e147.
- [32] A. Amran, et al., Solubility dynamic of methyl yellow and carbon black in microemulsions and lamellar liquid crystal of water, non ionic surfactants and cyclohexane system, in: *IOP Conference Series: Materials Science and Engineering*, IOP Publishing, 2016.
- [33] H. Kim, K. Park, M.-Y. Lee, Biocompatible dispersion methods for carbon black, *Toxicol. Rev.* 28 (4) (2012) 209.
- [34] A. Ghadimi, R. Saidur, H. Metselaar, A review of nanofluid stability properties and characterization in stationary conditions, *Int. J. Heat Mass Tran.* 54 (17) (2011) 4051e4068.
- [35] Z. Haddad, et al., A review on how the researchers prepare their nanofluids, *Int. J. Therm. Sci.* 76 (2014) 168e189.
- [36] R.A. Taylor, et al., Nanofluid optical property characterization: towards effi- cient direct absorption solar collectors, *Nanoscale Res. Lett.* 6 (1) (2011) 1e11.
- [37] A. Lenert, E.N. Wang, Optimization of nanofluid volumetric receivers for solar thermal energy conversion, *Sol. Energy* 86 (1) (2012) 253e265.
- [38] V. Khullar, et al., Solar energy harvesting using nanofluids-based concen- trating solar collector, *J. Nanotechnol. Eng. Med.* 3 (3) (2012) 031003.
- [39] H. Zhang, et al., Dependence of photothermal conversion characteristics on different nanoparticle dispersions, *J. Nanosci. Nanotechnol.* 15 (4) (2015) 3055e3060.
- [40] S.-Q. Zhou, R. Ni, Measurement of the specific heat capacity of water-based Al₂O₃ nanofluid, *Appl. Phys. Lett.* 92 (9) (2008) 093123.
- [41] W.M. Rohsenow, J.P. Hartnett, Y.I. Cho (Eds.), *Handbook of HeatTransfer*, third ed., McGraw- Hill, 1998, p. 2.26.